Semiconductor Optoelectronics
ISSN: 1001-5868

THE INFLUENCE OF THE INTERNAL STRUCTURE OF BIMETALLIC NANOPARTICLES ON THE OPTICAL PROPERTIES OF AUAG/GLASS MATERIAL

Ali Nasir Abdul Hussein
Ministry of Education, Iraq

Abstract
Multiple-sphere T-matrix approach is used to examine the optical extinction spectra of nanoparticles. These nanoparticles have different alloy structures, shell-like nature, inverse ""core-shell"" architectures, metal concentrations. A unique approach for determining the architecture of nanoparticles (whether they have a "core-shell" structure or are alloyed) using just information about A place for “"plasmon resonance"” and creating the parts we need is suggested by examining simulations and existing literature.
The work finds that the internal structure of monodisperse non-interacting "bimetallic nanoparticles" with a known may be effectively determined across a large range of possible configurations by using the optical spectrum fitting technique. However, the approach encounters difficulties and constraints in precisely characterizing the internal structure of nanoparticles larger than 60 nm in radius and containing fewer than about 25% silver atoms.
Overall, the research highlights the potential of using optical extinction spectra analysis and fitting techniques to unravel the structural properties of nanoparticles, but acknowledges certain limitations for specific nanoparticle sizes and compositions
Keyword: Optical extinction spectra**,** Nanoparticles**,** Metal concentrations**,** Architectural configurations**,** "plasmon resonance"

Introduction:

Nanoparticles of silver and gold have attracted significant attention in the field of research, particularly in the study of their optical properties. These nanoparticles are often embedded within dielectric matrices, such as glass, and exhibit both linear and nonlinear optical phenomena. These optical properties are primarily attributed to phenomenon known as localized surface "plasmon resonance" ("SPRL"). [1-3]
These nanoparticles' Capacity, appearance, atomic composition, level agglomeration, and the dielectric characteristics of the surrounding matrix all affect how they behave optically. The wavelength at which surface photoluminescence ("SPRL") occurs is significantly influenced by the size and form of the nanoparticles. The optical response of the nanoparticles can be altered by adjusting these factors.
Since the contribution of the "SPRL" to the optical spectrum may be separated from interbond transitions, there is special interest in the situation of gold and silver nanoparticles embedded in glass. The plasmonic characteristics of these nanoparticles may now be understood and used with more precision because to this separation. Plasmonic nanoparticles can restrict

electromagnetic radiation on a scale lower than its wavelength by taking use of the "SPRL" effect. Applications in photonics and optoinformatics depend on this feature.

Plasmonic nanoparticles have already found applications in various fields. For example, they are used in spectroscopy techniques for studying single molecules and nanoscale objects. The ability to localize electromagnetic radiation allows for enhanced sensitivity and resolution in these spectroscopic measurements. Furthermore, plasmonic nanoparticles hold promise for other applications in areas such as sensing, imaging, and light manipulation

In addition to the advancements in controlling the size and shape of nanoparticles, recent developments in nanotechnology have also focused on the internal structure of nanoparticles. This means that are not only manipulating the external geometry but also exploring variations in the arrangement of atoms within the nanoparticles.

While in "bimetallic nanoparticle" mode, a particularly interesting approach It is the main structure configuration. These structures involve combining two different types of metals within a single nanoparticle, Where one of them will be the foundation and the second will be the perimeter. This configuration is often represented as AB, where A represents the metal in the core and B represents the metal in the shell.

The "core-shell" structure provides unique properties and functionalities that are different from those of single-component nanoparticles. By carefully selecting the metals for the core and shell, can tailor the physical and chemical properties of the nanoparticles to meet specific requirements. The choice of metals can influence factors such as catalytic activity, stability, and optical properties. [7-9]

The "core-shell" structure offers several advantages. For example, the shell can act as a protective layer, shielding the core from the environment, preventing oxidation, and enhancing These parts go to calm. Its architecture also allows for additional control over the interactions between the nanoparticles and their surroundings. This control is crucial for applications such as catalysis, sensing, and energy conversion.

Furthermore, the synthesis of "core-shell" nanoparticles involves precise control over the growth process, including the deposition of one metal onto the core material. Techniques such as chemical reduction, galvanic replacement, and seed-mediated growth are commonly employed to achieve the desired "core-shell" structures

This makes it possible to modify the morphology of the bimetallic nanoparticles in gold-silver nanoparticles in order to regulate the material's optical properties, electrochemical deposition [10,11], and pure chemical approaches.

Another promising method co-sputtering technique, where metal and substrate materials are simultaneously deposited onto a surface [12]. This method leads to the formation of materials that contain bimetallic nanoparticles, and these nanoparticles exhibit changes in their optical properties.

One interesting phenomenon observed in these materials is the shift in the wavelength of the "plasmon resonance". "plasmon resonance" refers to the collective oscillations of electrons in a metal nanoparticle in response to incident light. The presence of two different metals, such as silver and gold, in the bimetallic nanoparticles can cause variations in the "plasmon resonance" wavelength compared to nanoparticles composed of a single metal. This shift in the optical spectrum provides valuable information about the composition and structure of the nanoparticles.

However, determining the exact structure and architecture of the synthesized nanoparticles can be challenging. The internal structure of the nanoparticles can vary, ranging from an ideal "core-shell" structure with distinct core and shell regions to a more homogeneous alloy-like structure where the two metals are uniformly mixed. Experimental characterization techniques may not provide a detailed understanding of the nanoparticle structure at the atomic level.

This is where theoretical methods come into play. Theoretical approaches and computational simulations play a significant role in bridging the gap between the observed optical properties and the underlying structural features of the material. By employing theoretical models and simulations, can study the electronic and optical properties of different nanoparticle configurations and compare them with experimental data. These methods help in deducing the most likely structures and architectures adopted by the bimetallic nanoparticles

"plasmon resonance" spectra can be theoretically described at several levels: continuum models of nanoparticles, effective electrical LC circuit models [15–17]. The most widely used techniques are continuum methods, are used to introduce information on the metallic nanoparticles' nature and, less frequently, their surroundings. These functions are based on observed dielectric constants of bulk samples [4,22,23], and can be provided in tabular or analytical forms [19–21]. An effective size-dependent dielectric function ε (ω, D), which accounts for the variations in nanoparticle electronic structure relative to bulk materials, should be used when evaluating particles smaller than about 10 nm [15, 24]. Although there have been created analytical modifications to the bulk dielectric function [21, 25], we will restrict our analysis to particles larger than 10 nm, where size effects in the dielectric permittivity can be disregarded.

Notable methods among the continuum approaches are the discrete dipole methods [28, 29], finite difference [26], and finite element [27]. These methods may describe particles of any shape, but they become problematic when many arbitrarily positioned particles are taken into account [30]. Mie theory gives quantitative explanations of size dependence and makes local field distributions calculable [31–33]. The T-matrix technique [36–38] and generalized multiparticle Mie theory (GMM) [34, 35] can be used to extend Mie theory to many spheres, including "core-shell" structures. The T-matrix technique has a high computing efficiency, which is advantageous when investigating plasmonic materials, especially for randomly oriented particle clusters.

The T-matrix method has been successfully applied in a number of instances to the study of both ordered arrays and diluted particle systems, including dimers, linear chains, spherical layers, ellipsoids, nanorods, and nanodisks [39–41]. We have recently shown that this method is applicable to the investigation [42]. which may be explained within classical frameworks, has been investigated rather well; nevertheless, little is known about the optical properties of bimetallic particles. The GMM approach was used in a recent work [43] to theoretically investigate the optical spectra of nanoparticles with "core-shell" configurations such as Ag Au and Au Ag. It was shown that the shell-to-core radius ratio affected the plasmon peak's location, while the impact of particle size on its plasmonic characteristics received less consideration. Furthermore, the case of alloy-type nanoparticles, which is practically significant, was overlooked.

A homogeneous alloy structure (Au1−xAgx), an Ag core Au shell (AgAu), and three different nanoparticle sizes (small /16 nm/, medium /30 nm/, big about /60 nm/ are all taken into

consideration in this study. The impact of two-particle plasmon interactions on the "plasmon resonance" spectrum is seen in Section 3.3. The prospect of resolving the inverse problem of recreating the structure of the nanoparticle from its optical spectrum is investigated in Section 3.4. A succinct synopsis of the results is given in Section 4, the conclusion.

2. Theoretical Methods:

We built a Python module [42, 45] to operate the Multi-Spheres T-matrix (MSTM) program [44], which was used to calculate the optical extinction spectra of spherical particle systems. The T-matrix method, (fv) in terms of regular vector spherical harmonics to the scattered field's expansion coefficients (aμ) in terms of outgoing spherical harmonics.

$$a_\mu = \sum_\nu T_{\mu\nu} f_\nu, \qquad (1)$$

Where /n = [1 ÷ ∞[/, m = /−n ÷ n/, and /p = 1, 2/ are the three values that each index μ and ν represents. Tμν represents the T-matrix's components. The limit on the value of n in (1) is n_{max} < 10 for numerical computations. The T-matrix components are analytically stated in terms of the Mie theory coefficients when dealing with a single sphere. One must solve the equations related to the dispersion mechanism in order to derive the dispersion matrix T for a multi-domain system. Calculating the scattering and absorption coefficients of the system as well as calculating the average over all directions with respect to the incident radiation with high computational efficiency is made possible by knowing the T matrix of the system.

The dielectric functions of bulk materials described by the Drude-Lorentz model with analytical modifications developed in [46] were the dielectric functions of materials used as nanoparticles.

$$\varepsilon(\omega, x) = \varepsilon_\infty(x) - \frac{\omega_p^2(x)}{\omega^2 + i\omega\Gamma_p(x)} + \varepsilon_{CP1}(\omega, x) + \varepsilon_{CP2}(\omega, x), \qquad (2)$$

ω_p and Γ_p are the Drude model's plasma frequency and energy width, εCP1 and εCP2 are the interband transition-related contributions to the dielectric permittivity, and ε∞ is the high-energy transition-related contribution. The authors of [46] chose the parameters in equation (2) to characterize experimental data for films made of gold, silver, and their alloys.
$Au1{-}_xAg_x$ (x = 0.33, 0.5, 0.67).

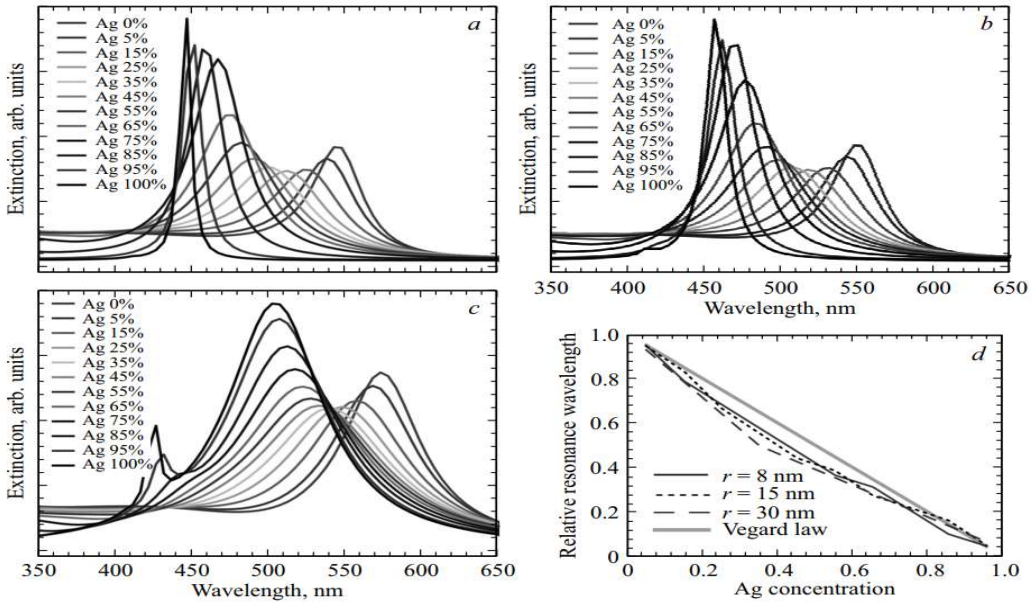

Fig. 1. " Optical endpoint colocalization of Au1−x Agx alloy-structured nanoparticles, where the radius is /a/ — /8/, /b/ — /15/, and/ c/ — /30/ nm, and the quantity of silver x varies. The linear law that corresponds to Vegard's rule and the concentration dependence of the "plasmon resonance" peak position are shown in the inset (d).".

3. Results and Conclusions:

3.1. "Nanoparticles" with the structure of an unordered solid solution:

The work focuses on nanoparticles with a homogeneous mixing of silver and gold atoms within an unordered solid solution structure. In this instance, the alloy's dielectric function can be used to characterize the optical characteristics of the nanoparticles. investigated nanoparticles having radii of 8 nm, 15 nm, and 30 nm (Figures 1a, 1b, and 1c). The nanoparticles' silver content ranged from 0% to 100% in 5% increments.

In the obtained spectra shown in Fig. 1a-c, a single peak is observed, except for large particles with high silver content.

Additionally, the shape of the peak is noticeably affected by both size and composition variations. These variations can provide valuable information for structural analysis based on optical spectra. By analyzing the shape and position of the peak, can gain insights into the composition and structure of the nanoparticles, including the mixing ratio of silver and gold atoms.

For clarity, the spectra shown in Fig. 1a-c for particles with a silver content above 85% have been reduced by a factor of 2 to 5. This reduction helps in visualizing the overall trends and characteristics of the spectra

To evaluate data such as the band gap, Vegard's empirical rule [47] is often used, which creates an increasing curve between the isotropy and the atomic concentration. Applying this rule to estimate the plasmon resonance wavelength, assuming that the sizes of the nanoparticles are equal, we obtain the equation:

$$\lambda^{\text{Vegard}}(x, R) = (1 - x)\lambda_{\text{Au}}(R) + x\lambda_{\text{Ag}}(R), \qquad (3)$$

where λAu (R) and λAg (R) are the "plasmon resonance" wavelengths with radius /R/, and x is concentration silver atoms. accuracy in this instance is readily confirmed by looking at the locations of the peaks on the curves that the MSTM computed.

$$\Lambda = \frac{\lambda - \lambda_{\mathrm{Au}}(R)}{\lambda_{\mathrm{Ag}}(R) - \lambda_{\mathrm{Au}}(R)}. \qquad (4)$$

In this case, the prediction according to Vegard's rule can be described by the function 3Vegard(x) = 1 - x, which is independent of size, which is under consideration bears a close approximation as shown in Figure 2

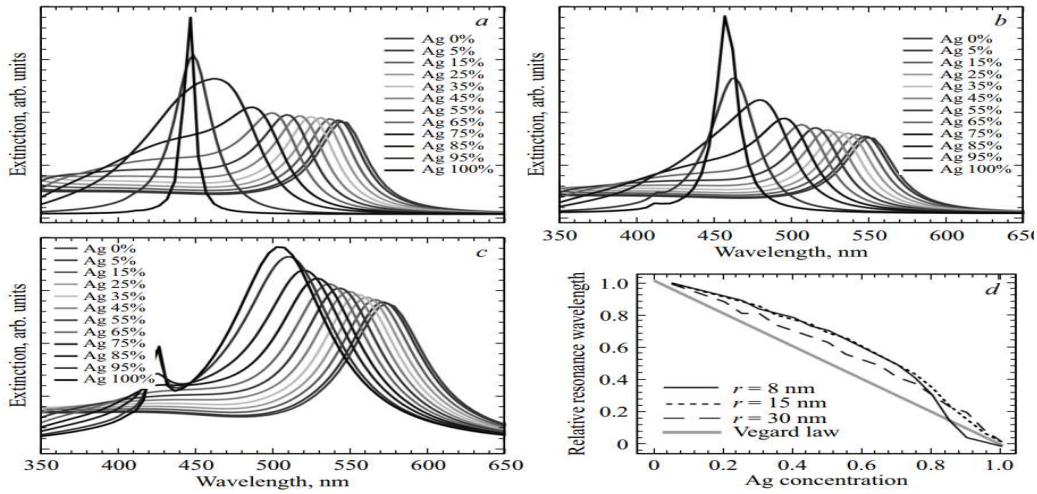

Fig. 2". AuAg "core-shell" nanoparticles with varied (/a - 8 nm/, /b – 15/ nm, and c - /30 nm/) and variable silver concentration (x) have their optical extinction spectra calculated. The linear law that corresponds to Vegard's rule and the concentration dependency of the plasmon peak position are shown in Insert (d)."

The "relative" plasmon peak wavelengths are presented on the vertical axis. However, the values predicted by Vegard's rule are systematically overestimated.

3.2. "core-shell" Nanoparticles:

In this study, examined "core-shell" nanoparticles, where a core of one metal (gold) is surrounded by a shell of another metal (silver). The same parameterization of the dielectric function used for the alloy nanoparticles was applied here, considering the pure metal phases of gold and silver for the core and shell, respectively. However, the limiting concentration values were defined as x = 0 for gold and x = 1 for silver, indicating that the core is made of pure gold and the shell is made of pure silver.

Particles were considered. However, instead of varying the silver concentration, the changed the radius of the gold core while keeping the overall size of the nanoparticle's constant. The optical extinction spectra of the "core-shell" nanoparticles were then calculated.

The acquired optical extinction spectra for gold core and silver shell (Au Ag) "core-shell" nanoparticles are displayed in Fig. 2a–c. Furthermore, the spectra for the "reverse" structure, in which silver is in the core and gold is on the surface, are shown in Fig. 3a–c (Ag Au).

To facilitate comparison, the intensity plots of the spectra for particles with a silver content exceeding 85% were reduced by a factor of 2 to 5. This reduction in intensity allows for clearer visualization of the overall trends and features of the spectra.

By examining the optical extinction spectra of these "core-shell" nanoparticles with varying gold core radii and silver shell compositions, can gain insights into how the arrangement and composition of the core and shell materials influence the optical properties of the nanoparticles. This knowledge is crucial for understanding the plasmonic behavior and potential applications of such "core-shell" structures in various fields, including sensing, imaging, and energy conversion.

The computed spectra of "core-shell" structures (Figs. 2 and 3) show a somewhat more complex structure than that of alloys: the primary peak becomes less symmetrical and an extra "shoulder" form to the left of it. Nevertheless, when particle size increases and silver content falls, this effect diminishes.

As in the preceding section, the dependencies of the "plasmon resonance" position on the concentration of silver in "core-shell" nanoparticles are depicted in Figs. 2d and 3d. As predicted, in contrast to the case of alloy structures, there is a significantly larger departure from the linear trend, which corresponds to Vegard's rule. It is noteworthy that consistent variations from Vegard's rule occur at silver concentrations below approximately 75%, which contrast with the aberrations shown in the alloy example (Fig. 1d).

The behavior of "plasmon resonance" shifts can serve as a distinguishing factor between "core-shell" structures and alloy structures, even without conducting additional calculations, given that the particle sizes and metal concentrations are known. This observation is supported by experimental findings presented in study [48]. In this study, gold-silver nanoparticles with a well-defined silver concentration and an approximate size of 10 nm were synthesized.

The positions of the "plasmon resonance" peaks in the experimental optical spectra were found to be located above the line predicted by Vegard's rule. Vegard's rule states that the lattice constant of a solid solution varies linearly with the alloy composition. The deviation from Vegard's rule in the experimental data suggests a significant influence of alloying and component diffusion within the nanoparticles.

These experimental observations were further confirmed by transmission electron microscopy (TEM) data obtained in the same study. The TEM images provided visual evidence of the presence of "core-shell" structures and demonstrated the non-uniform distribution of the metal elements within the nanoparticles.

Based on these results, the authors of study [48] concluded that the observed deviations from Vegard's rule indicate a substantial alloying effect and diffusion of the metal components in the nanoparticles. This implies that the nanoparticles exhibit characteristics of alloy structures rather than pure "core-shell" configurations.

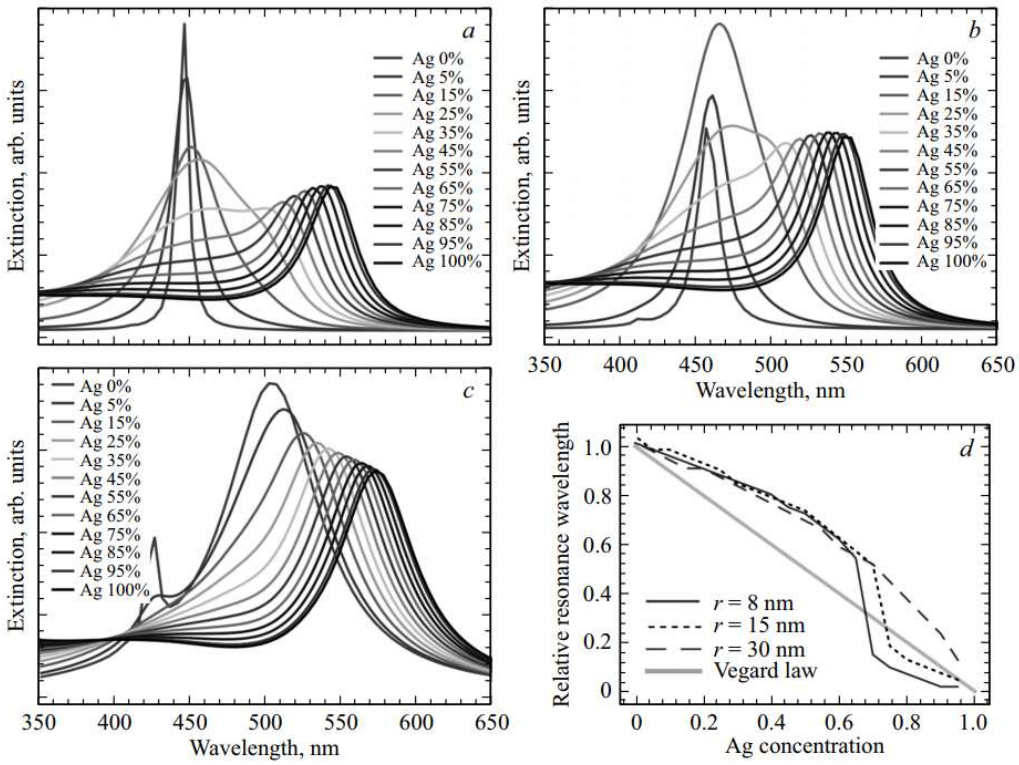

Fig. 3. "AgAu "core-shell" nanoparticles with varied radii (a - 8 nm, b - 15 nm, and c - 30 nm) and silver concentrations (x) had their optical extinction spectra calculated. The linear trend that corresponds to Vegard's rule and the concentration dependencies of the "plasmon resonance" peak position are depicted in Insert (d)."

3.3. Influence of particle-particle interactions on the optical extinction spectrum:

Plasmon coupling, the term for the alteration of the extinction spectrum caused by interactions between nearby particles, can cause the electromagnetic field to be redistributed [4]. Figure 4 presents estimated spectra for a system of two 10 nm AuAg nanoparticles with interparticle gaps of 3, 5, and 16 nm to demonstrate the effect of plasmon coupling on the optical spectrum of "core-shell" nanostructures. When the gap size between the particles rises, the spectra's qualitative behavior resembles that of monometallic particles [4, 42].

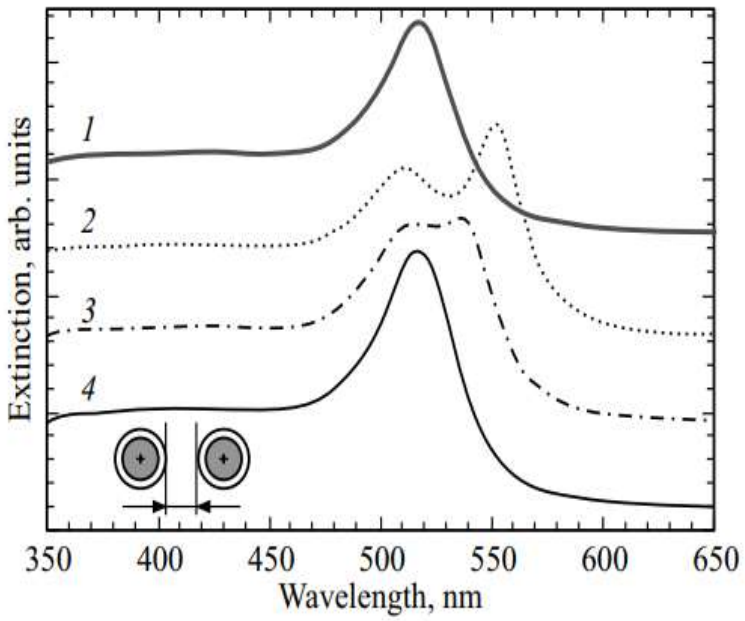

Fig. 4. " Extinction optical spectra of three similar particles: two with a gap width of three (2), five (3), and sixteen nm (4), and one Au@Ag particle (curve 1). The nanoparticles' radius is 10 nm ."

A discernible reorganization of the PPR spectrum takes place for particles whose radius is smaller than the particle; this is indicated by the emergence of a new peak and a displacement of the principal peak (curves 2 and 3 in Fig. 4). The spectral shape nearly matches with that of an isolated particle when the interparticle gap width is roughly equal to or greater than the particle radius (curves 1 and 4 in Fig. 4).

Approximate maximum interparticle gap width for the considered nanoparticles is 1.6 times the particle radius, which is an intermediate value between the characteristic values for gold and silver nanoparticles (approximately 1.4 and 2.4 times the radius, respectively) at which plasmonic interaction becomes indistinguishable.

3.4 Uniqueness of the solution to the inverse scattering problem:

Figures 1-3 demonstrate the similarities and differences between the optical extinction spectra of nanoparticles with various topologies. Asymmetry of primary peaks and the development of extra maxima are distinguishing characteristics, while shifts in "plasmon resonance" and peak lengths are commonalities.

This raises the question of whether optical spectrum analysis can be used to fundamentally discriminate between different nanoparticle designs. However, this problem is theoretically ill-posed and the uniqueness of the solution cannot be guaranteed because it is a subset of the inverse scattering problem.

Numerous fittings have been done in order to answer this question, especially for non-interacting monodisperse bimetallic particles. These fitters used models of alternate architectures, such as alloy configurations, "core-shell", and inverse "core-shell", to fit spectra

estimated for nanoparticles with a known architecture.

In these fittings, a number of factors were adjusted, such as the background constant and scaling factor, particle size, core radius for "core-shell" particles, and silver concentration for alloy particles. This method is comparable to the one that reference [42] describes.

A comparison of curves was done between 350 and 800 nm in wavelength, which includes the major "plasmon resonance" peak and its surrounding region, in order to calculate the minimal misfit function.

The fitting results for AuAg nanoparticles with radii of 9, 15, and 46 nm and silver concentrations of 47%, 65%, and 22%, respectively, are shown in Figure 5. The "unknown" fitted function was the nanoparticles' spectra.

These numbers were chosen from tens of fits that were carried out using various parameters to determine the fitted function. Figure 5c demonstrates that the three architectures under consideration are identical when dealing with large particles that have low metal contents, particularly when it comes to "core-shell" and inverse "core-shell" configurations. The spectra of small and medium-sized nanoparticles, however, cannot be fully fitted (Figures 5a-b), suggesting that resolution may be achievable.

(Note: Certain statistics and their contents are mentioned in the original text, which cannot be faithfully conveyed in text form. As a result, the description offered is a broad interpretation of the meaning of the text.

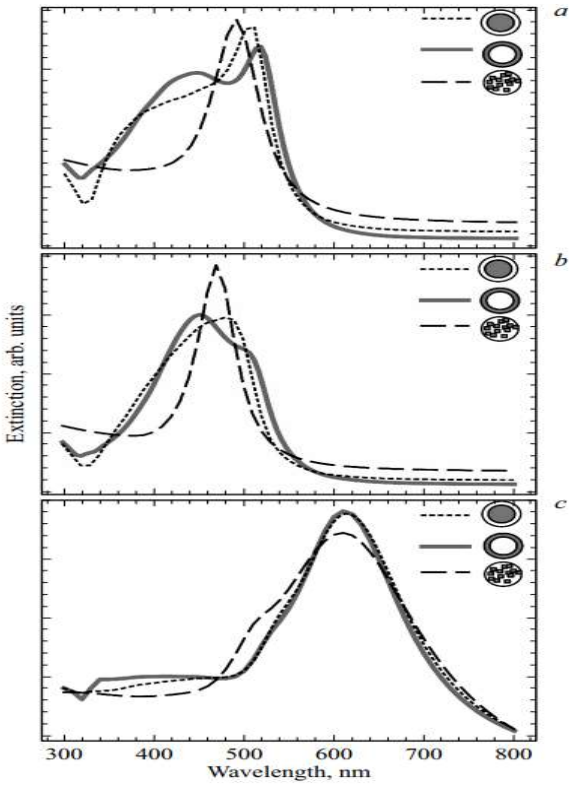

Figure 5" demonstrates the fitting outcomes of the optical extinction spectra of single nanoparticles with a thick gray line representing the "core-shell" AgAu structure, with radii of 9 nm (a), 15 nm (b), and 46 nm (c) and silver concentrations of 47%, 65%, and 25%, respectively. Au-Ag alloy (dashed line) and "inverse" "core-shell" AgAu (dots) are the alternative structural models that are taken into consideration"

To conduct a more thorough analysis of nanoparticle architecture, it is crucial to consider additional factors such as the particle size distribution and the influence of plasmonic interactions among the particles.

Firstly, the size distribution of nanoparticles plays a significant role in their optical properties. Nanoparticles within a sample can have varying sizes, leading to variations in the "plasmon resonance" behavior and peak widths. Incorporating the size distribution information into the analysis allows for a more accurate representation of the optical spectra.

Secondly, plasmonic interactions between nanoparticles can have a considerable impact on their collective optical response. These interactions occur when nanoparticles are in close proximity to each other, leading to coupling effects and modifications in the overall spectra. It is important to take into account these interactions and understand their influence on the observed optical extinction spectra.

In summary, when analyzing nanoparticle architecture, a comprehensive examination should involve considering the particle size distribution and the effects of plasmonic interactions among the particles. This broader approach will provide a more detailed understanding of the optical properties and help distinguish between different nanoparticle architectures.

4. Conclusions:

Based on the calculations of optical extinction spectra and comparison with literature data, several conclusions can be drawn:

1. Regardless of whether gold-silver nanoparticles are alloyed or have a "core-shell" structure, changing their composition allows for a broad range adjustment of the "plasmon resonance" position. Because of their tunability, the nanoparticles' optical characteristics can be altered to fit a variety of uses.
2. Depending on the nanoparticle architecture, the concentration dependency of the "plasmon resonance" wavelength changes considerably. The opposite deviations are shown when using Vegard's rule, which determines the "plasmon resonance" position based on composition. The estimation tends to be underestimated for "core-shell" and inverse "core-shell" designs with silver concentrations below about 75%, and overstated for alloy-like nanoparticles. With the use of optical spectra and information on the composition of the material, this feature can be used to determine the implemented architecture.
3. The plasmon interaction length of bimetallic nanoparticles lies between the corresponding features of monometallic nanoparticles. Accordingly, the optical response of the nanoparticles is affected by the presence of two metals and the spatial extent of plasmon coupling.
4. Generally speaking, a fitting procedure with different structural models can be used to accurately identify the structural parameters of non-interacting monodisperse

nanoparticles over a wide range of wavelengths (from 350 to 800 nm). However, working with very large particles (radii larger than about 60 nm) and low silver concentrations (less than about 25%) presents difficulties and uncertainty.

These results emphasize how crucial it is to take into account the size, content, and design of nanoparticles when examining optical extinction spectra. They also highlight the possibility of customizing nanoparticles' optical characteristics for particular uses.

References:

[1] D.J. de Aberasturi, A.B. Serrano-Montes, L.M. Liz-Marzan. Adv. Opt. Mater. **3**, 602 (2015). DOI:10.1002/adom.201500053

[2] И.А. Гладких, Т.А. Вартанян. Оптика и спектроскопия **121**, 916 (2016); [I.A. Gladskikh, T.A. Vartanyan. Opt. Spectroscopy **121**, 851 (2016).] DOI: 10.1134/S0030400X16120109

[3] V. Amendola, R. Pilot, M. Frasconi, O.M. Marago, M.A. Iati. J. Phys.: Condens. Matter. **29**, 203002 (2017).

[4] U. Kreibig, M. Vollmer. Opt. Properties of Metal Clusters. "SPRl"inger (1995). 553 c.

[5] T. Hartman, C.S. Wondergem, N. Kumar, A. van den Berg, B.M. Weckhuysen. J. Phys. Chem. Lett. **7**, 1570 (2016). DOI: 10.1021/acs.jpclett.6b00147

[6] L.-B. Luo, K. Zheng, C.-W. Ge, Y.-F. Zou, R. Lu, Y. Wang, D.- D. Wang, T.-F. Zhang, F.-X. Liang. Plasmonics **11**, 619 (2016). DOI: 10.1007/s11468-015-0091-3

[7] R. Ghosh Chaudhuri, S. Paria. Chem. Rev. **112**, 2373 (2012). DOI: 10.1021/cr100449n

[8] V. Guterman, S. Belenov, A. Pakharev, M. Min, N. Tabachkova, E. Mikheykina, L. Vysochina, T. Lastovina. Int. J. Hydrogen Energy. **41**, 1609 (2016). DOI: http://dx.doi.org/10.1016/j.ijhydene.2015.11.002

[9] T. Dang-Bao, D. Pla, I. Favier, M. Gomez. Catalysis **7**, (2017). DOI: 10.3390/catal7070207

[10] L. Lu, G. Burkey, I. Halaciuga, D.V. Goia. J. Colloid Interface Sci. **392**, 90 (2013). DOI: https://doi.org/10.1016/ j.jcis.2012.09.057

[11] J. Haug, H. Kruth, M. Dubiel, H. Hofmeister, S. Haas, D. Tatchev, A. Hoell. Nanotechnology **20**, 505705 (2009).

[12] Г.Н. Макаров. Успехи физических наук **183**, 673 (2013); [G.N. Makarov. Phys. Usp. **56**, 643 (2013).] DOI: 10.3367/UFNr.0183.201307a.0673

[13] J. Deng, J. Du, Y. Wang, Y. Tu, J. Di. Electrochem. Commun. **13**, 1517 (2011). DOI: 10.1016/j.elecom.2011.10.010

[14] P. Dong, Y. Lin, J. Deng, J. Di. ACS Appl. Mater. Interfaces **5**, 2392 (2013). DOI: 10.1021/am4004254

[15] S.M. Morton, D.W. Silverstein, L. Jensen. Chem. Rev. **111**, 3962 (2011). DOI: 10.1021/cr100265f

[16] S. Bernadotte, F. Evers, C.R. Jacob. J. Phys. Chem. C **117**, 1863 (2013). DOI: 10.1021/jp3113073

[17] P. Koval, F. Marchesin, D. Foerster, D. Sanchez-Portal. J. Phys.: Condens. Matter. **28**, 214001 (2016).

[18] Н.А. Олехно, Я.М. Бельтюков, Д.А. Паршин. ФТТ **57**, 24052414 (2015). [N.A. Olekhno, Y.M. Beltukov, D.A. Parshin. Phys. Solid State **57**, 24792488 (2015).] DOI: 10.1134/S1063783415120252

[19] A. Alabastri, S. Tuccio, A. Giugni, A. Toma, C. Liberale, G. Das, F.D. Angelis, E.D. Fabrizio, R.P. Zaccaria. Materials **6**, 4879 (2013). DOI: 10.3390/ma6114879
[20] P. Jahanshahi, M. Ghomeishi, F.R.M. Adikan. Sci. World J. **2014**, 6 (2014). DOI: 10.1155/2014/503749
[21] A. Derkachova, K. Kolwas, I. Demchenko. Plasmonics (Norwell, Mass.) **11**, 941 (2016). DOI: 10.1007/s11468-015-0128-7
[22] C. Sonnichsen, T. Franzl, T. Wilk, G. von Plessen, J. Feldmann. New J. Phys. **4**, 93 (2002).
[23] X. Fan, W. Zheng, D.J. Singh. Light Sci. Appl. **3**, e179 (2014).
[24] A. Crut, P. Maioli, F. Vallee, N.D. Fatti. J. Phys.: Condens. ´ Matter. **29**, 123002 (2017).
[25] S. Berciaud, L. Cognet, P. Tamarat, B. Lounis. Nano Lett. **5**, 515 (2005). DOI: 10.1021/nl050062t
[26] A. Taflove, S. Hagness. Computational Electrodynamics: The Finite-difference Timedomain Method. Artech House (2005). 1038 c.
[27] J. Jin. The Finite Element Method in Electromagnetics. Wiley (2015) 876 c.
[28] B.T. Draine, P.J. Flatau. J. Opt. Soc. Am. A **11**, 1491 (1994). DOI: 10.1364/JOSAA.11.001491
[29] P.J. Flatau, B.T. Draine. Opt. Express **20**, 1247 (2012). DOI: 10.1364/OE.20.001247
[30] O. Zhuromskyy. Crystals **7**, 1 (2017). DOI: 10.3390/cryst7010001
[31] W. Haiss, N.T.K. Thanh, J. Aveyard, D.G. Fernig. Anal. Chem. **79**, 4215 (2007). DOI: 10.1021/ac0702084
[32] P.N. Njoki, I.-I.S. Lim, D. Mott, H.-Y. Park, B. Khan, S. Mishra, R. Sujakumar, J. Luo, C.-J. Zhong. J. Phys. Chem. C **111**, 14664 (2007). DOI: 10.1021/jp074902z
[33] M. Heinz, V.V. Srabionyan, A.L. Bugaev, V.V. Pryadchenko, E.V. Ishenko, L.A. Avakyan, Y.V. Zubavichus, J. Ihlemann, J. Meinertz, E. Pippel, M. Dubiel, L.A. Bugaev. J. Alloys Compd. **681**, 307 (2016). DOI: http://dx.doi.org/10.1016/j.jallcom.2016.04.214
[34] Y.-L. Xu. Appl. Opt. **34**, 4573 (1995). DOI: 10.1364/AO.34.004573
[35] G. Gouesbet, G. Grehan. J. Opt. A **1**, 706 (1999).
[36] P.C. Waterman. Proc. IEEE. **53**, 805 (1965). DOI: 10.1109/PROC.1965.4058
[37] M.I. Mishchenko. J. Opt. Soc. Am. A**8**, 871 (1991). DOI: 10.1364/JOSAA.8.000871
[38] D.W. Mackowski, M.I. Mishchenko. J. Opt. Soc. Am. A**13**, 2266 (1996). DOI: 10.1364/JOSAA.13.002266
[39] N.G. Khlebtsov. J. Quant. Spectrosc. Rad. Transfer. **123**, 184 (2013). DOI: http://dx.doi.org/10.1016/j.jqsrt.2012.12.027
[40] M.I. Mishchenko, N.T. Zakharova, N.G. Khlebtsov, G. Videen, T. Wriedt. J. Quant. Spectrosc. Rad. Transfer. **178**, 276 (2016). DOI: 10.1016/j.jqsrt.2015.11.005
[41] M.I. Mishchenko, N.T. Zakharova, N.G. Khlebtsov, G. Videen, T. Wriedt. J. Quant. Spectrosc. Rad. Transfer. **202**, 240 (2017). DOI: http://dx.doi.org/10.1016/j.jqsrt.2017.08.007
[42] L. Avakyan, M. Heinz, A. Skidanenko, K.A. Yablunovskiy, J. Ihlemann, J. Meinertz, C. Patzig, M. Dubiel, L. Bugaev. J. Phys.: Condens. Matter. **30**, 045901 (2018). DOI: 10.1088/1361-648X/aa9fcc
[43] C. Zhang, B.-Q. Chen, Z.-Y. Li, Y. Xia, Y.-G. Chen. J. Phys. Chem. C **119**, 1683616845 (2015).
DOI: 10.1021/acs.jpcc.5b04232
[44] D. Mackowski, M. Mishchenko. J. Quant. Spectrosc. Rad. Transfer. **112**, 2182 (2011).

DOI: 10.1016/j.jqsrt.2011.02.019
[45] L.A. Avakyan. Python wrapper for multiple sphere *T* -matrix (MSTM) code to calculate surface "plasmon resonance" ("SPRL") spectrum, (2017). https://github.com/lavakyan/mstmspectrum
[46] D. Rioux, S. Vallieres, S. Besner, P. Munoz, E. Mazur, M. Meunier. Adv. Opt. Mater. **2**, 176 (2014).
DOI: 10.1002/adom.201300457
[47] A.R. Denton, N.W. Ashcroft. Phys. Rev. A **43**, 3161 (1991). DOI: 10.1103/physreva.43.3161
[48] S. Ristig, O. Prymak, K. Loza, M. Gocyla, W. Meyer-Zaika, M. Heggen, D. Raabe, M. Epple. J. Mater. Chem. B **3**, 4654 (2015). DOI: 10.1039/c5tb00644a

.